Journal of Power Sources 195 (2010) 7278–7288

Contents lists available at ScienceDirect

Journal of Power Sources

journal homepage: www.elsevier.com/locate/jpowsour

Three-dimensional numerical simulation of water droplet emerging from a gas diffusion layer surface in micro-channels

Y. Ding, H.T. Bi*, D.P. Wilkinson

Department of Chemical and Biological Engineering, University of British Columbia, Clean Energy Research Centre, 2360 East Mall, Vancouver, BC, V6T 1Z3, Canada

ARTICLE INFO

Article history:
Received 20 March 2010
Received in revised form 29 May 2010
Accepted 31 May 2010
Available online 8 June 2010

Keywords:
PEM fuel cell
Two-phase flow
Mini channels
VOF simulation

ABSTRACT

The dynamic formation of water droplets emerging from a gas diffusion layer (GDL) surface in micro-channels was simulated using the volume of fluid (VOF) method. The influence of GDL surface microstructure was investigated by changing the pore diameter and the number of pore openings on the GDL surface. Simulation results show that the microstructure of the GDL surface has a significant impact on the two-phase flow patterns in gas flow channels. For a non-uniform GDL surface, three stages were identified, namely emergence and merging on the GDL surface, accumulation on the channel sidewalls and detachment from the top wall. It was also found that if the pore size is small enough, the flow pattern in the channel does not change with further reduction in the pore diameter. However, the two-phase flow patterns change significantly with the wettability of the GDL surface and sidewalls, but remain the same when the liquid flow rate is reduced by two orders of magnitude from the reference case.

© 2010 Elsevier B.V. All rights reserved.

1. Introduction

Fuel cells, which directly convert chemical energy into electricity, show great potential as an alternative energy-conversion device. Although there are many types of fuel cells distinguished by the different electrolyte used, polymer-electrolyte membrane fuel cells (PEMFCs) have been receiving the most attention for their lower operating temperature (60–90 °C), simpler design and lower cost. Water management is a key issue to improve the performance of PEMFCs during the operation. The membrane should be well humidified to maintain high ionic conductivity, but, excess liquid water, i.e., flooding, should be avoided, because it blocks the diffusion pathway of reactants, causing a negative effect on the performance. The existence of liquid water in the flow channel also causes a higher pressure drop, resulting in increased parasitic energy loss. Thus, it is important to understand gas–liquid two-phase flow behaviors in PEMFCs channels in order to avoid severe flooding of the electrodes and mini flow channels.

Mathematical modeling and computational simulation are powerful tools to understand the two-phase flow in PEM fuel cells due to their low cost and easy implementation. Since 2000, two-phase models have begun to be incorporated into fuel cell modeling [1]. Several reviews on two-phase flow models and their applications in PEM fuel cells have been published in recent years [1–5]. Early two-phase flow models always assumed the liquid water moving at the same velocity as the gas flow, i.e., mist flow (e.g. [6,7]). However, in situ experimental results showed that at high current densities, water emerged from preferential sites on the GDL surface forming droplets rather than mists [8]. Other two-phase flow models, e.g. mixture model [9] and multi-fluid model [10,11], are widely used in modeling two-phase phenomena in PEM fuel cells, but are not able to capture the liquid droplet shape. In recent years, the volume of fluid (VOF) method has become popular in modeling gas–liquid flow in PEM fuel cell channels due to its capacity to consider surface tension and wall adhesion effects and its ability to track the interface between the two phases. Therefore, liquid droplet behaviors can be captured explicitly. Several modeling papers based on the VOF method have been published with both droplet formation and motion being investigated. [8,12,13] Parametric studies on the effects of material wettability, gas or liquid velocity, contact angle hysteresis and surface tension have also been reported [12,14–19]. Novel channel designs have also been tested by the VOF method [20–23]. VOF method was even coupled with electrochemical reaction, heat transfer and species transport to model a PEM fuel cell unit [24,25]. However, most work only focus on single droplet behavior or several droplets initially located in the gas channel; but none have considered the effects of microstructure of the GDL surface. The GDL surface has been treated either as a homogenous surface or a surface with only 1-pore opening for liquid water injection into the channel. The two-phase flow pattern in the flow channels of a real operating fuel cell is likely quite different from that determined based on droplets emerging from a uniform GDL surface, or from single droplet behavior. Therefore, it is essential to consider the microstructure effects of GDL surface

* Corresponding author. Tel.: +1 604 822 4408; fax: +1 604 822 6003.
E-mail address: xbi@chbe.ubc.ca (H.T. Bi).

0378-7753/$ – see front matter © 2010 Elsevier B.V. All rights reserved.
doi:10.1016/j.jpowsour.2010.05.059

while investigating gas–liquid two-phase flow patterns in PEMFCs channels.

Full consideration of detailed microstructure of the GDL, the so-called pore-scale model, needs extremely large computational time, and has been only employed for very small length scale systems [26–32]. The effect of GDL microstructure on the two-phase flow pattern in the gas flow channel is still poorly understood. In the present work, we simplified the microstructure of the GDL by creating a number of representative pores on the 2D GDL surface. Droplet formation and motion were then simulated using the VOF method. Different GDL surface structures were then simulated by changing the pore size and pore number. Parametric studies were also conducted to investigate the effect of GDL and channel walls wettability and liquid velocity on the two-phase flow pattern and pressure drop through the flow channel.

2. Numerical model and boundary conditions

2.1. Numerical method

In the VOF method, immiscible fluids can be modeled by solving a single set of momentum equations and then the volume fraction of each phase and also the interface between phases are tracked throughout the domain. Conservation equations include,

Mass conservation is given by,

$$\frac{\partial \rho}{\partial t} + \nabla \cdot (\rho \vec{v}) = 0 \tag{1}$$

where for gas–liquid flow, the mixture density is defined as,

$$\rho = s_l \rho_l + s_g \rho_g \tag{2}$$

where s is the volume fraction of each phase with subscripts l and g representing water and air, respectively. The volume fraction of each phase is given by the following relationship,

$$s_l + s_g = 1 \tag{3}$$

Momentum conservation is given by,

$$\frac{\partial(\rho \vec{v})}{\partial t} + \nabla \cdot (\rho \vec{v}\vec{v}) = -\nabla p + \nabla \cdot (\mu(\nabla \vec{v} + \nabla \vec{v}^{\mathrm{T}})) + \rho \vec{g} \tag{4}$$

where p is static pressure and μ is the dynamic viscosity given by,

$$\mu = s_l \mu_l + s_g \mu_g \tag{5}$$

and the velocity of the mixture is defined as,

$$\vec{v} = \frac{s_l \rho_l \vec{v}_l + s_g \rho_g \vec{v}_g}{s_l \rho_l + s_g \rho_g} \tag{6}$$

Volume fraction conservation is given by,

$$\frac{\partial(s_l \rho_l)}{\partial t} + \nabla \cdot (s_l \rho_l \vec{v}) = 0 \tag{7}$$

The surface tension effect is considered by the continuum surface force (CSF) model proposed by Brackbill et al. [33]. In this model, extra surface tension results in a source term in the momentum equation (4) given by,

$$F_{\mathrm{vol}} = \sigma \left(\frac{\rho \kappa_l \nabla s_l}{1/2(\rho_l + \rho_g)} \right) \tag{8}$$

where σ is the surface tension coefficient, and κ_l is the surface curvature of the liquid droplet defined in terms of the divergence of the unit normal, $\vec{n}_l$ given by,

$$\kappa_l = \nabla \cdot \vec{n}_l \tag{9}$$

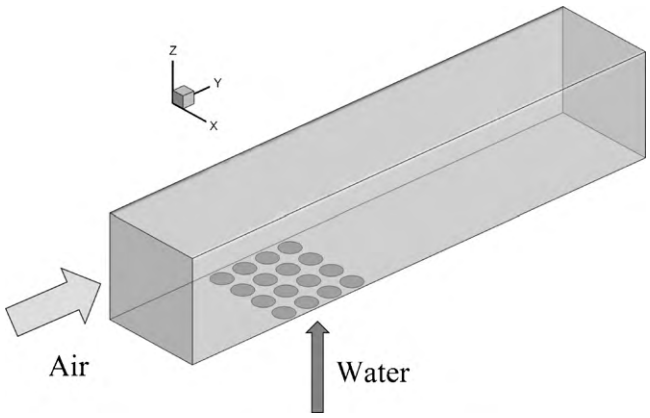

Fig. 1. Three-dimensional computational domain.

The unit normal, $\vec{n}_l$, is computed from local gradients in the surface normal at the interface.

$$\vec{n}_l = \frac{\nabla s_l}{|\nabla s_l|} \tag{10}$$

Wall adhesion effects are considered by adjusting the curvature of the surface near the wall, where the gas–liquid interface meets the solid surface. The local curvature of this interface is determined by the contact angle, θ_w, which is the angle between the wall and the tangent to the interface at the wall. The surface normal, $\vec{n}$, at the wall is given by,

$$\vec{n} = \vec{n}_w \cos\theta_w + \vec{t}_w \sin\theta_w \tag{11}$$

where $\vec{n}_w$ and $\vec{t}_w$ are the unit vectors normal and tangential to the wall, respectively.

The above governing equations are implemented in a commercial software, FLUENT® 6.3.26 [34]. The geometric reconstruction scheme of Youngs [35] is used to represent the interface between two fluids, which is the most accurate one for interface tracking [34].

2.2. Computational domain and Boundary Conditions

The three-dimensional computational domain is shown in Fig. 1. This cuboid channel which was used in all the simulations has a 250 μm × 250 μm square cross section and a 1250 μm length with a hydrophobic GDL surface on the bottom. Air flows into the channel from one end and liquid water was injected from several open pores on the GDL surface. For the base case, 16 pores were located within a 250 μm × 250 μm square on the GDL surface, each with a pore diameter of 50 μm, which corresponds to typical GDL surfaces with a porosity of 0.5 [36]. At the gas inlet, the velocity of air was set at 10 m s^{-1}, which is of the same order of magnitude as flows encountered in automotive fuel cell stacks [17]. The theoretical calculation of liquid generation rate for example at a current density of 800 mA cm^{-2} is 0.20 mg h^{-1}. However, in order to shorten the time for water accumulation in the channel, the liquid injection velocity was set at 0.0625 m s^{-1} for all the pores with a corresponding mass flow rate of 7 g h^{-1}. Quan and Lai reported [23] that deviations introduced by amplifying the water generation rate by several orders of magnitude are insignificant due to the large flow rate ratio between gas and liquid water. Laminar flow and no-slip boundary condition were assumed since the Reynolds number of each phase is quite small (Re_g = 171, Re_l = 7.8). The static contact angle for the GDL surface and channel wall surfaces were set at 140° and 45° respectively, based on typical values for PTFE treated carbon paper GDL materials [36]. There are two sidewalls and one top wall in the channel in addition to the bottom GDL surface. The time step for

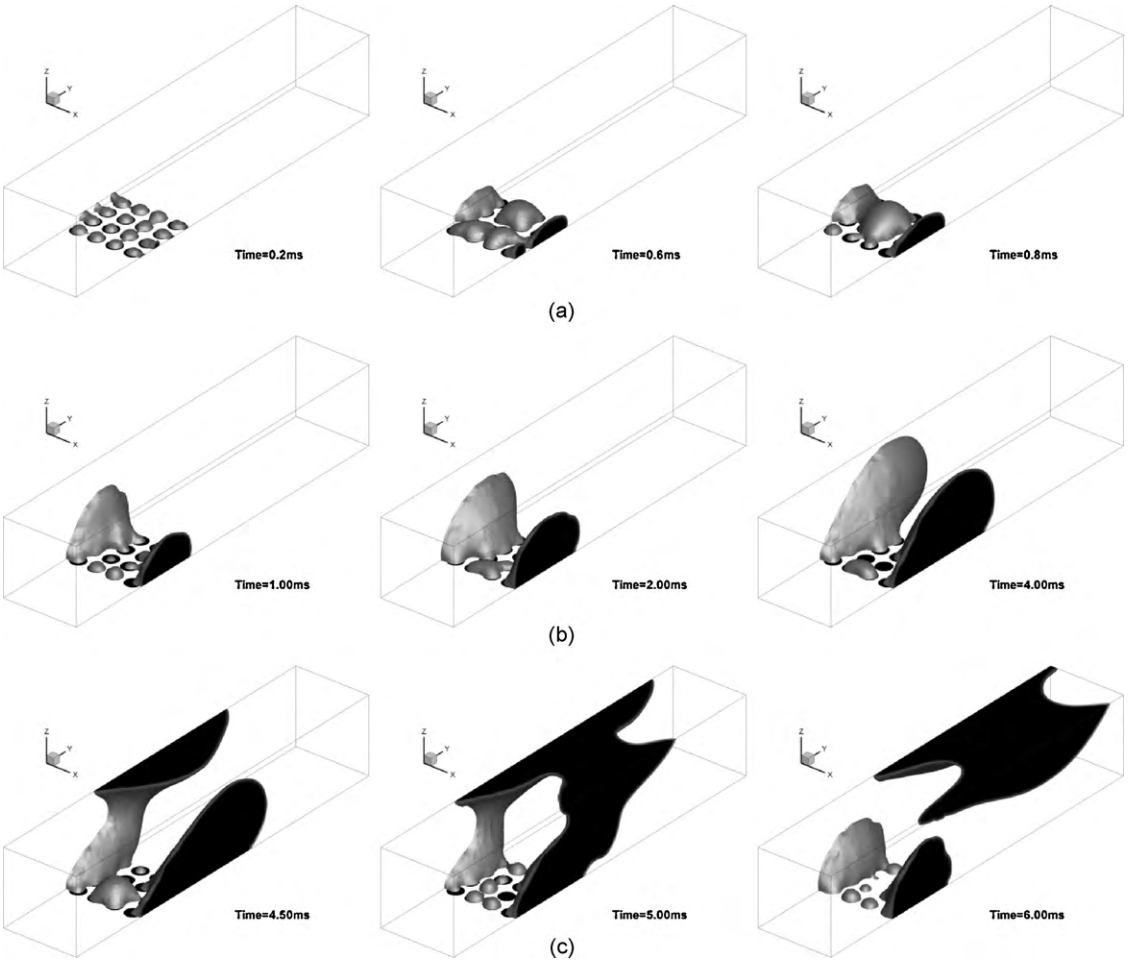

Fig. 2. Three stages of the emerging water droplet into a channel: (a) emergence and merging, (b) accumulation, and (c) detachment.

the baseline simulation was set at 10^{-7} s to ensure that the global courant number is less than one. The mesh size was set to 10 μm, with 82,625 meshes in total for the base case. Smaller mesh sizes, e.g. 8 μm and 5 μm, were also tested, and the results showed no obvious difference from the base case. Therefore, the mesh size for all the other cases was also set to 10 μm to save computational time.

3. Results and discussion

Due to small length scale of the channel, the surface tension effects were more noticeable. For base case conditions, the capillary number (Ca), the Weber number (We), and the Bond number (Bo) were much less than one, which means the surface tension force was the dominant force in comparison to the viscous force, inertia force, and gravity force in the mini flow channel.

3.1. Two-phase flow pattern evolution

Fig. 2 clearly shows three stages of two-phase flow pattern evolution in the channel: emergence and merging on the GDL surface, accumulation on the sidewall, and detachment on the top wall. In the emergence and merging stage, small droplets emerging from each pore coalesce on the GDL surface, which generates a liquid film covering the injection area. At the same time, liquid water is continually accumulating in the channel, and due to the wettability difference between the GDL surface and channel walls, liquid water tends to accumulate on the sidewalls which results in the formation of large droplets. As these droplets "grow" larger and larger, they begin to move slowly along the sidewalls. Once these droplets reach the top wall, the liquid water rapidly spreads on the top wall, resulting in a thin film on the top wall. As this liquid film moves outward quickly, some of water on the sidewall is also dragged away. In the last stage, the top liquid film detaches itself from the droplets on the sidewalls due to its faster speed, and a new cycle begins. It is worth noting that the emergence and merging stage and the accumulation stage occur continuously in the channel, but the detachment stage only occurs periodically.

These three stages of dynamic droplet behaviors can also be identified by the time evolution of the water coverage ratio on the different surfaces of the channel, the water volume fraction and the total pressure drop (Fig. 3). The water coverage ratio is defined as the ratio of the surface area covered by water to the total surface area. In PEM fuel cells, reactants diffuse through the GDL, hence, the GDL surface water coverage ratio is a key parameter that indicates the negative effects of liquid water on PEM fuel cell performance. The water volume fraction or degree of saturation indicates the degree of channel flooding. The pressure drop, which is another important parameter, indicates the energy loss of fluid flowing through the channel. For operating PEM fuel cells, a lower GDL surface water coverage ratio, a lower water fraction, and a lower pressure drop are preferred.

From Fig. 3, it can be seen that the water coverage ratio on the GDL surface continuously increases at the beginning (up to 4 ms), due to the emerging small droplets. At the same time, liquid water also accumulates on the sidewall, and the higher water coverage

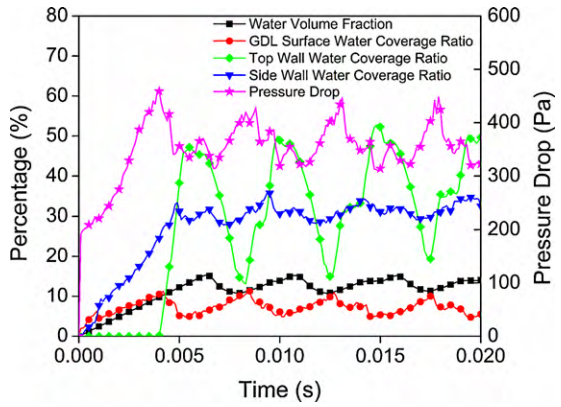

Fig. 3. Time evolution of water distribution and pressure drop.

on the sidewall is due to the different wettabilities between the sidewall and GDL the surface. The pressure drop also increases, corresponding to the increase in the water volume fraction. After about 4 ms, a sudden drop in the GDL surface water coverage ratio occurs, followed by a steep increase in the top wall water coverage ratio, indicating the droplet's fast spread to the top wall. The pressure drop also decreases rapidly, even though the level of water saturation is still increasing. This is because the buildup of droplets on the hydrophobic GDL surface occupies more cross-sectional area. On the other hand, water on the hydrophilic channel walls forms a thin film, which occupies much less cross-sectional area, imposing little influence on the pressure drop even though the volume of this liquid film is much higher than the droplets on the GDL surface. The liquid film on the top wall moves faster than the droplets on the sidewalls, and soon (at 5.5 ms) this film detaches from the droplet, resulting in a maximum top wall water converge ratio and a minimum GDL and sidewall water coverage ratio. Once the detached liquid film is flushed out of the channel, a new cycle begins. From the flow pattern shown in Fig. 3, it can be concluded that the pressure drop does not correspond to the level of water saturation, but to the size of the droplets located on the GDL surface. Thus, these results indicate that most empirical equations which correlate pressure drop with water fraction, should not be applied to PEM fuel cell channels.

3.2. Effects of water inlet structures

GDLs, which are typically fabricated from carbon fibers, connect catalyst layers and gas flow field and provide a pathway for electrons, gases, and liquid water to move to and from the catalyst layers. The microstructure of the GDL plays an important role in water management. In this section, several pore structures are simulated to examine the effect of the microstructure of the GDL surface on the flow patterns in order to identify a simple but representative structure for future use in the simulation of large-scale fuel cell stacks. Five structures, (uniform inlet, 1-pore inlet, 4-pore inlet, 16-pore inlet, and 64-pore inlet), with the same open area and liquid flow rate, were selected and are shown in Fig. 4.

The uniform inlet case (Fig. 4a) is a commonly used approximation in many CFD simulations. For this case, the microstructure of the GDL is neglected, and a very distinct two-phase flow pattern is observed in the channel, as shown in the three snapshots of flow pattern evolution in Fig. 5a. Only one big droplet is formed during

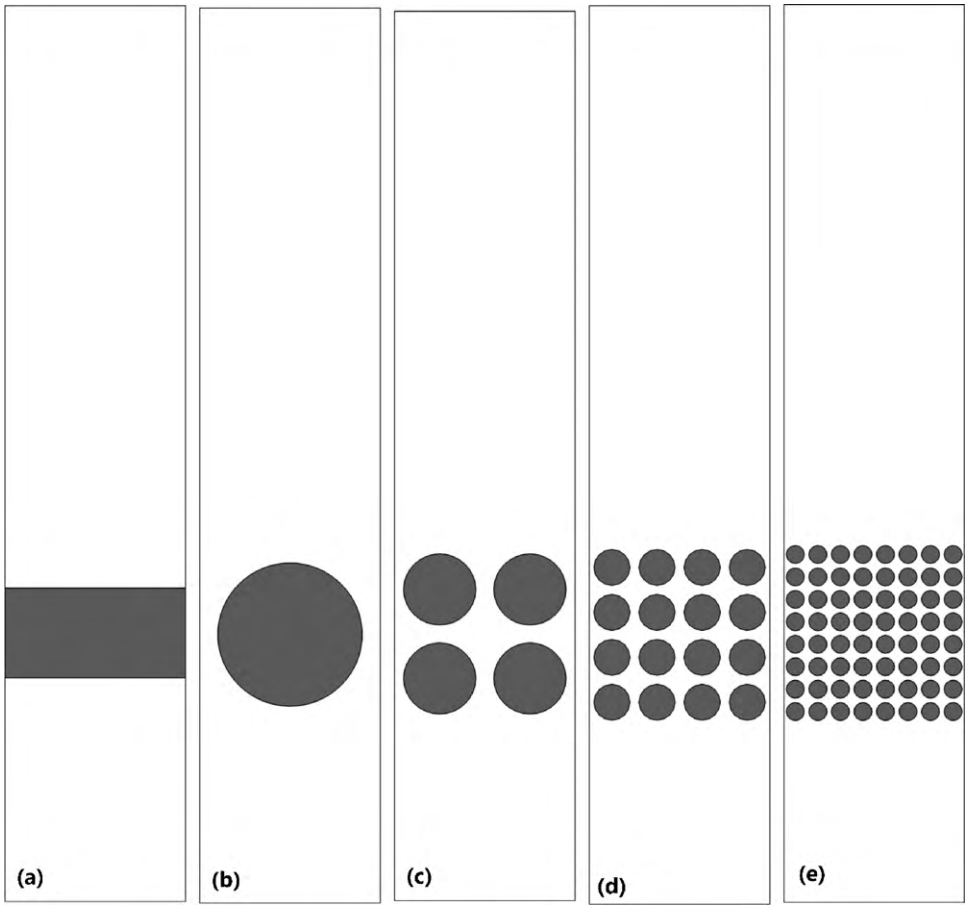

Fig. 4. Different water injection inlet structures representing the GDL: (a) uniform, (b) 1-pore, (c) 4-pores, (d) 16-pores (base case), and (e) 64-pores.

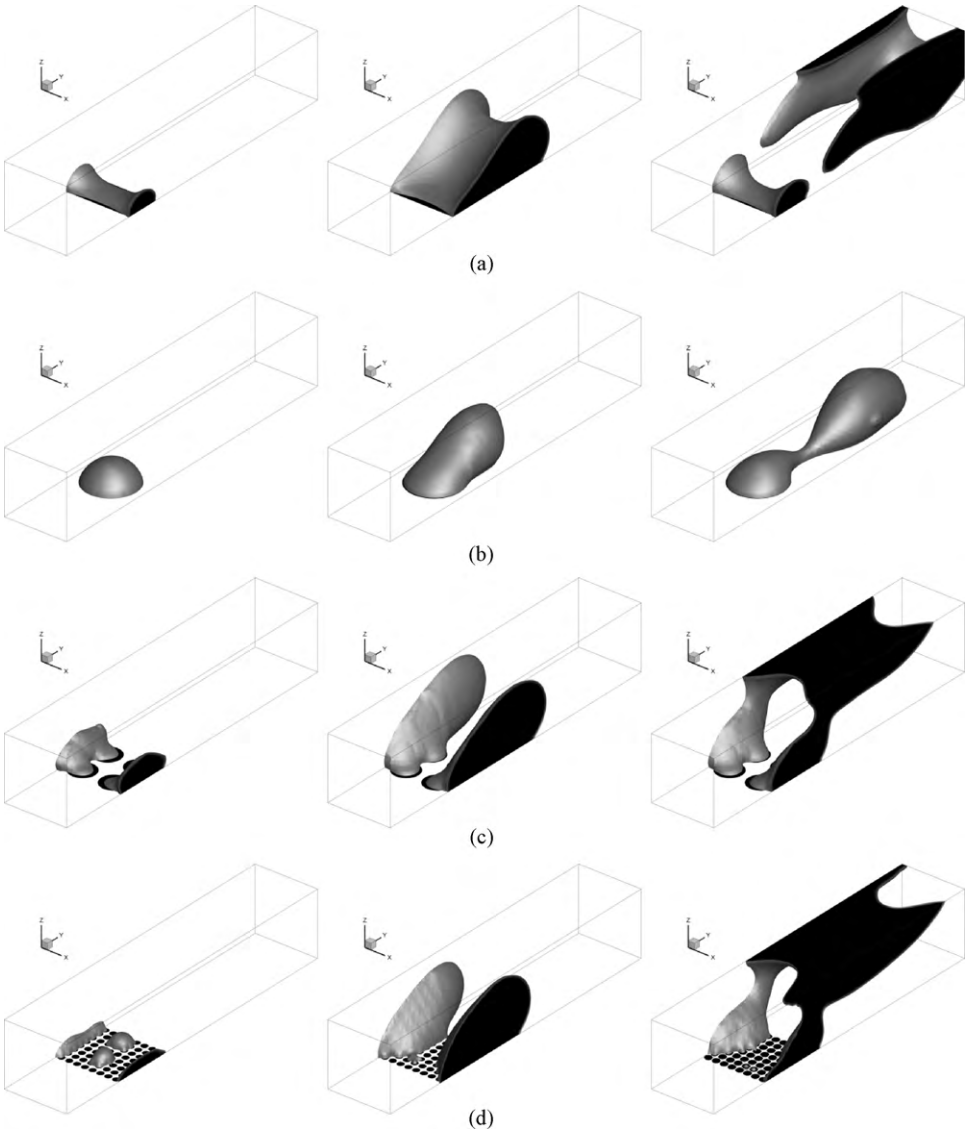

Fig. 5. Effects of water inlet configurations on the two-phase flow patterns: (a) uniform, (b) 1-pore, (c) 4-pore, and (d) 64-pore.

the merging stage, and the liquid accumulation occurs simultaneously on the GDL surface and sidewalls. As a result, more liquid stays on the hydrophobic GDL surface, which slows down the droplet spread on the hydrophilic sidewalls and makes the liquid droplet detach before it reaches the top wall, leading to the formation of liquid slugs. The 1-pore case (Fig. 4b) is another commonly used configuration to investigate the droplet behavior in PEM fuel cell micro-channels. Similar to the uniform inlet case (Fig. 5b), only one droplet forms in the channel. However, this droplet is not big enough to touch either the sidewalls or the top wall before detach-

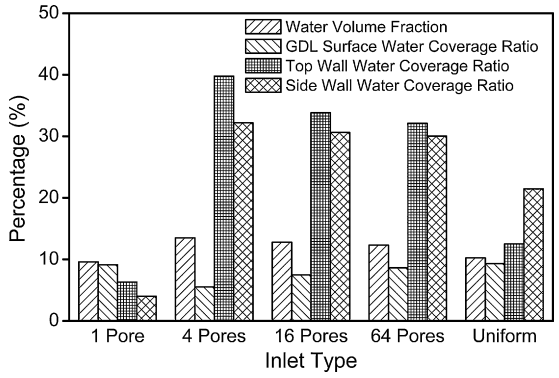

Fig. 6. Effects of water inlet configurations on the time-averaged water distribution.

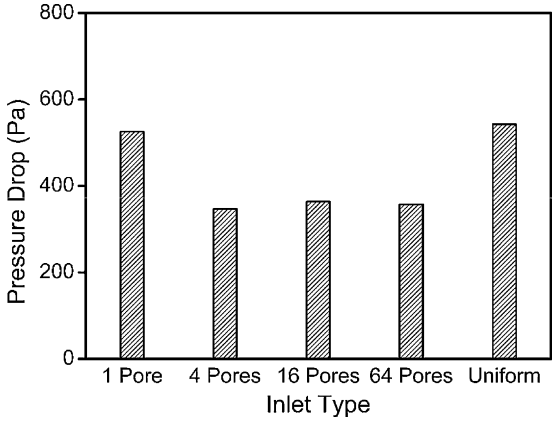

Fig. 7. Effects of water inlet configurations on the time-averaged pressure drop.

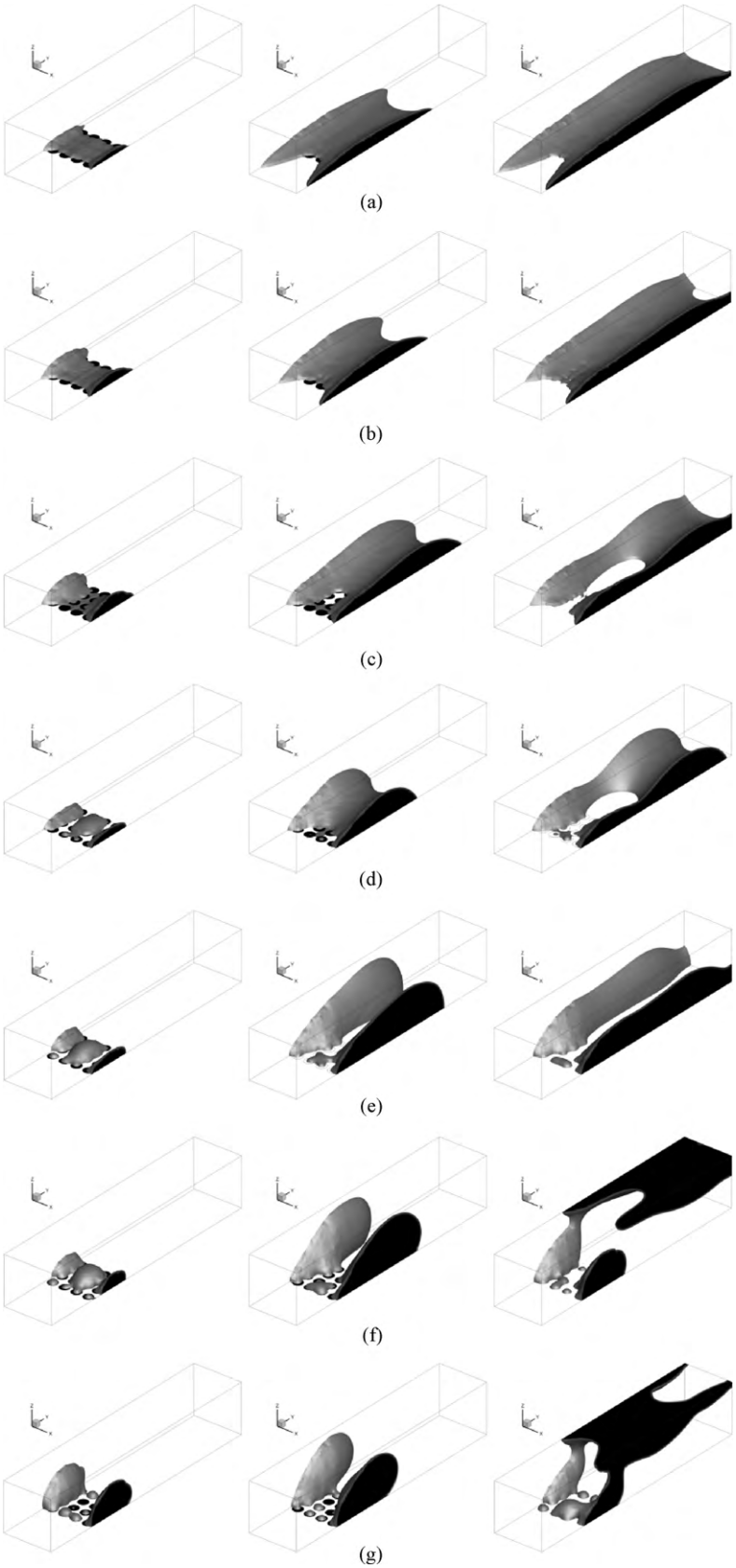

Fig. 8. Effects of GDL surface wettabilities on the two-phase flow patterns: (a) $\theta = 0^\circ$, (b) $\theta = 30^\circ$, (c) $\theta = 45^\circ$, (d) $\theta = 60^\circ$,(e) $\theta = 90^\circ$, (f) $\theta = 120^\circ$, and (g) $\theta = 180^\circ$.

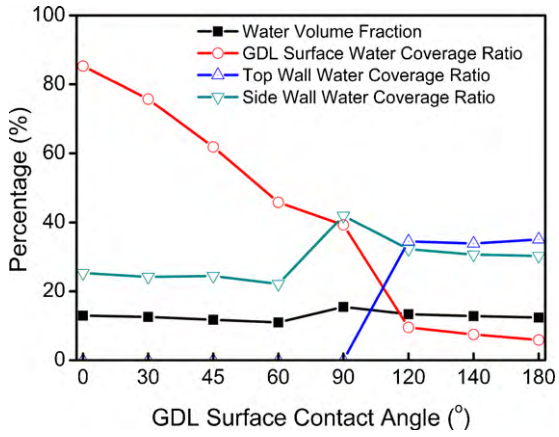

Fig. 9. Effects of GDL surface wettabilities on time-averaged water distribution.

ment, leading to droplet flow in the channel. The two-phase flow patterns with 4 pores and 64 pores (Fig. 5c and d) are very similar to the case with 16 pores, with three stages of water dynamic behavior present.

The effects of pore structures on the flow patterns can also been seen clearly from the time-averaged water distribution shown in Fig. 6. The uniform inlet and 1-pore cases have a higher water coverage ratio on the GDL surface and a much lower coverage ratio on the channel walls, compare to the 4-pore and 64-pore cases which have very similar water distribution with the base case of 16 pores due to the similar two-phase flow pattern in the channel. The effects of pore structures on the time-averaged pressure drop are shown in Fig. 7. The uniform inlet and 1-pore inlet cases show a much greater pressure drop than the three multi-pore cases which have a lower and similar pressure drop. As discussed previously, the pressure drop is dominated by water residing on the GDL surface, which creates more blockage of the gas channel than water on the other channel walls. Thus, the pressure drop of both the uniform inlet and 1-pore cases is much higher, which results in faster liquid removal, and thus lower average water volume fraction in the flow channel, as shown in Fig. 6.

In a real fuel cell, droplets emerge from preferential sites on the GDL surface. At the front of the channel, small droplets are formed and the flow pattern is mainly droplet flow as shown in the 1-pore case. As these small droplets move along the channel, droplets coalesce and form larger droplets which are able to touch sidewalls. As a result, the flow pattern in this region would be similar to that shown by the multiple pore cases. Since the GDL pores are quite small and non-uniform in size, and the pores are randomly distributed on the GDL surface, a full consideration of the detailed microstructure of the GDL surface is almost impossible. However, the previous cases demonstrate that when the pore size is small enough (e.g. 4-pore case), the flow pattern changes little with a further increase in the number of pores or a reduction in the pore diameter. Thus, the 4-pore case could be considered as a minimum required number of pores in order to capture the two-phase flow pattern in the fuel cell mini channel at a reasonable computational time demand.

3.3. *Effects of GDL surface contact angles*

The wettability of the GDL, which is characterized by the surface contact angle, can be altered by varying the PTFE content of the GDL. Although the GDL wettability has been shown to have a significant impact on the liquid water transport inside the GDL [37], its impact on the two-phase flow pattern in the gas channel is still unclear. In this section, the effects of GDL surface wettability on the flow pattern in the mini channel were investigated by varying the water/GDL surface static contact angle from 0° to 180°, i.e., 0°, 30°, 45°, 60°, 90°, 120°, and 180°. Fig. 8 shows different two-phase flow patterns in channels for different GDL wettabilities. When the GDL surface contact angle is less than that of sidewalls (Fig. 8a and b), a thin liquid film forms on the GDL, which covers almost all of the GDL surface. For a hydrophilic GDL surface with a contact angle less than 90° (Fig. 8c–e), a liquid water film still tends to be formed. This liquid film blocks the diffusion pathway of gas reactants to the catalyst layer, leading to decreased fuel cell performance. Since the GDL is hydrophilic, some water may even flow back from the channel towards the catalyst layer, which would further decrease the fuel cell performance. As the contact angle of the GDL surface increases, liquid water begins to accumulate on the sidewalls, and the higher the contact angle, the more water moves from the GDL surface to the sidewalls. When the GDL surface is hydrophobic with a contact angle greater than 90° (Fig. 8f and g), liquid water droplets form on the GDL surface, and grow until they are detached. It should be noted that the flow patterns on hydrophobic GDL surfaces are all similar to the base case in Section 3.1.

Fig. 9 shows that hydrophobic and hydrophilic GDL surfaces show very different liquid distribution profiles. For the hydrophilic GDL surface, the water coverage ratio on the sidewalls changes very little with varying GDL contact angle, and no water is present on the top wall, but the water coverage ratio on the GDL surface decreases significant as the contact angle increases. That is because a higher contact angle lifts the water up, i.e., move from a film to a droplet, which is more conducive to water removal from the GDL surface. For the hydrophobic GDL surface, the water coverage ratio on both the GDL and side/top surfaces changes little with varying the GDL contact angle, and a the stable flow pattern is formed as observed in the base case. It is worth to note that for 90° case, the water coverage ratio on the GDL surface is similar to that of hydrophilic GDL surface but the water coverage ratio on the sidewall is close to that of hydrophobic GDL surface, indicating that the flow pattern for this case is in a transition state. The contact angle is big enough to lift up the water, leaving less water on the GDL surface, but the lift is not sufficient to make the liquid to reach the top wall. As a result, the water coverage ratio on the sidewall is the highest among all the cases.

The time-averaged water volume fraction is also shown in Fig. 9. For both hydrophilic and hydrophobic GDL surfaces, the water volume fraction decreases a little with an increase in contact angle. For a hydrophilic GDL surface, the liquid water is more in the form of a film. Increasing the GDL contact angle lifts up the water more from the GDL surface to occupy more cross-sectional channel area, hence facilitating liquid water being flushed out of the channel. For a hydrophobic GDL surface, the flow pattern is similar to the

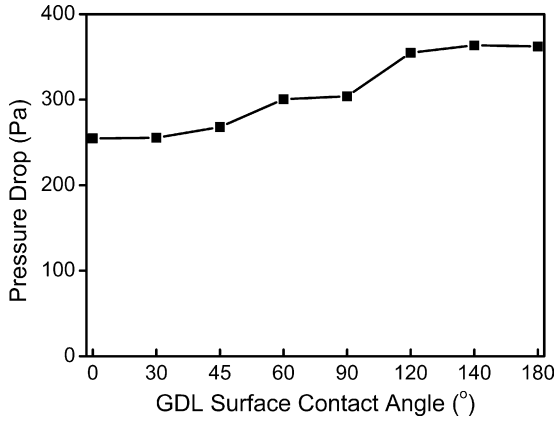

Fig. 10. Effects of GDL surface wettabilities on time-averaged pressure drop.

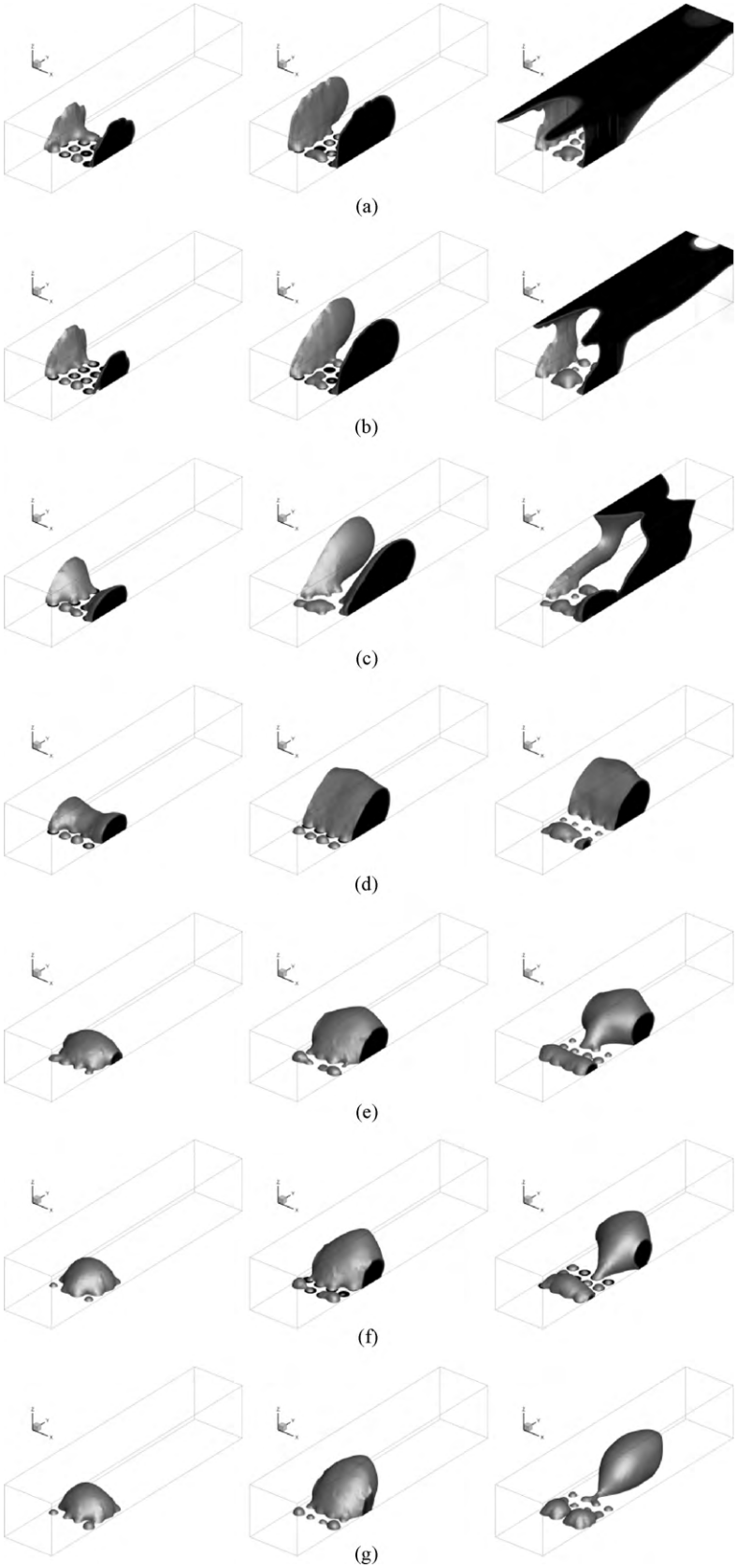

Fig. 11. Effects of channel wall wettabilities on two-phase flow patterns: (a) $\theta = 0^\circ$, (b) $\theta = 30^\circ$, (c) $\theta = 60^\circ$, (d) $\theta = 90^\circ$,(e) $\theta = 120^\circ$, (f) $\theta = 140^\circ$, and (g) $\theta = 180^\circ$.

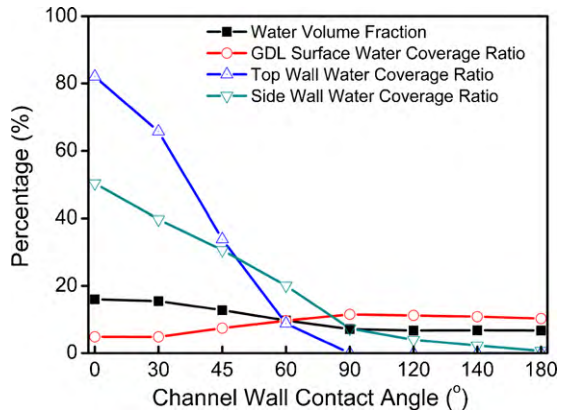

Fig. 12. Effects of channel wall wettabilities on time-averaged water distribution.

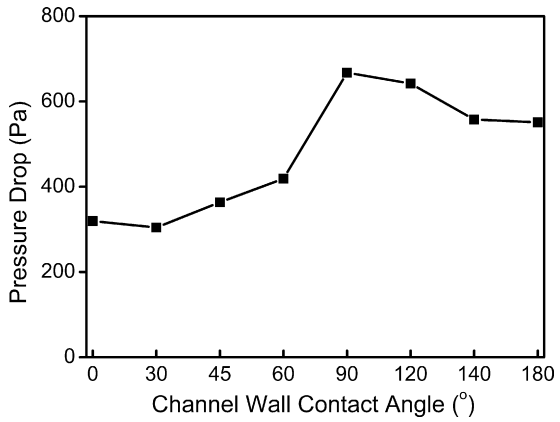

Fig. 13. Effects of channel wall wettabilities on time-averaged pressure drop.

base case, where increasing the contact angle helps the developing droplet to reach the top wall, which also facilitates the liquid water being flushed out of the channel. The corresponding time-averaged effects of GDL wettability on pressure drop is shown in Fig. 10. As discussed previously, the pressure drop is mainly caused by the liquid blockage of the gas channel. Thus, increasing the GDL surface contact angle should always increase the pressure drop. For the hydrophobic GDL surface, however, the pressure drop varies little with increasing the contact angle, since the water coverage ratio on the GDL surface almost remains the same as shown in Fig. 9.

It can be concluded from the above observation that increasing the hydrophobicity of the GDL surface is helpful to expel liquid water from the GDL surface and also reduce the water fraction in the channel, although the pressure drop only increases slightly. The wettability of the GDL also affects the water transport inside the GDL. Thus, It is difficult to conclude whether high or low wettability is beneficial for water management in the whole fuel cell system without coupling the mass transfer and electrochemical reactions into the hydrodynamics.

3.4. Effects of channel wall surface contact angles

Instead of changing the GDL surface wettability, one can also change the channel wall wettability for a given GDL to improve the water management in the gas channel. The effects of channel wall surface wettability were investigated by varying the water/wall surface static contact angle from 0° to 180°. Fig. 11 shows the effects of different wall surface contact angles, i.e., 0°, 30°, 45°, 60°, 90°, 120°, and 180°, on the two-phase flow pattern. For hydrophilic wall surfaces, three-stage flow patterns similar to the base case are observed. More hydrophilic wall surfaces make the droplet on the GDL easier to move to the top wall, and also decrease the thickness of the liquid film on both side and top walls. For hydrophobic wall surfaces, the flow pattern is similar to that of the 1-pore case with the droplet flowing on the GDL surface only and more hydrophobic wall surface prevents the formation of big droplets.

The effects of channel wall surface wettability on water distribution is shown in Fig. 12. As discussed previously, the more hydrophobic channel walls suppress liquid water removal from the GDL surface. As a result, the water coverage ratio on the top and sidewalls always decreases with increasing channel wall contact angle. Although the water volume fraction in the channel is higher for the more hydrophilic channel wall, the water coverage ratio on the GDL is smaller, resulting in more area for the gas reactants to diffuse through the GDL, leading to improved fuel cell performance. The pressure drop with different channel wall wettabilities (Fig. 13) also suggests that a more hydrophilic channel wall should be used in fuel cells to reduce the energy loss.

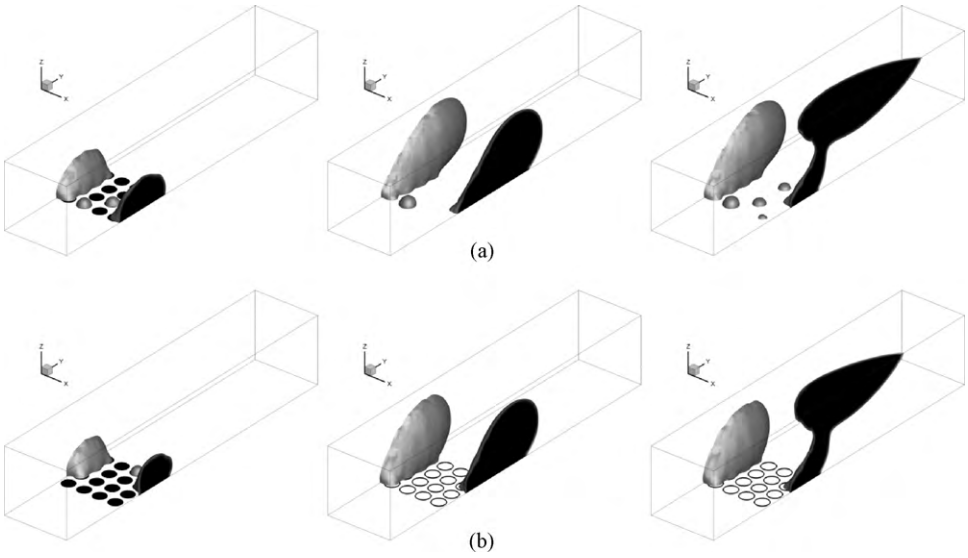

Fig. 14. Effects of liquid flow rates on two-phase flow patterns: (a) 1/10th, (b) 1/100th.

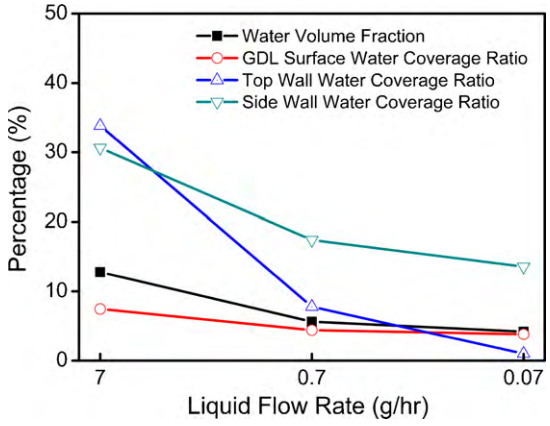

Fig. 15. Effects of liquid flow rates on time-averaged water distribution.

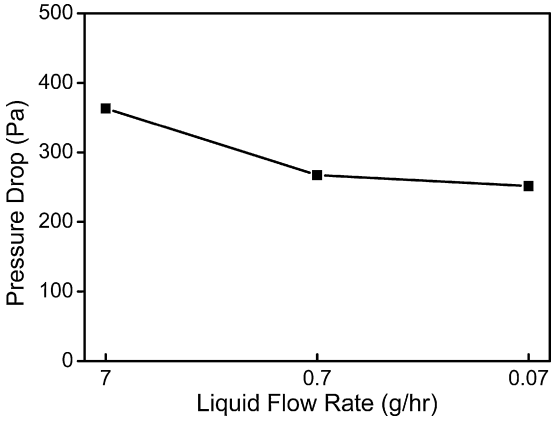

Fig. 16. Effects of liquid flow rates on time-averaged pressure drop.

3.5. *Effects of liquid flow rates*

As specified in the boundary conditions section, the liquid flow rate used in the base case simulation, i.e., 7 g h^{-1}, is much higher than the theoretical values according to the reaction rates, e.g. 0.2 mg h^{-1}. The effects of liquid flow rates were thus investigated in order to make sure the previous simulation results reveal the flow patterns in a real PEM fuel cell. In this section, two cases with liquid flow rate reduced to 10% and 1% of base case flow rate are investigated. Simulation results shown in Fig. 14 indicate the three-stage flow pattern remains the same even when the liquid flow rate is reduced by two orders of magnitude.

Water distribution with respect to liquid flow rates in Fig. 15 also shows that a lower liquid flow rate only results in a lower water coverage ratio on the top and sidewalls, but has little influence on the water coverage ratio on the GDL surface. This is because at the lower liquid flow rate, the liquid accumulation rate on the sidewalls is much smaller, and the adhesive force between top wall liquid thin film and sidewall droplets becomes weaker, which makes the droplet detachment from the top wall much easier. As a result, the water coverage ratio on the top and sidewalls decreases rapidly due to the relatively rapid removal of liquid water from the top wall. Correspondingly, the time-averaged water volume fraction and time-averaged pressure drop (Fig. 16) also become lower.

4. Conclusions

The following conclusions can be drawn from this simulation study:

(1) For a microstructured GDL surface, three stages of two-phase flow patterns can be identified when water is injected through the GDL into the gas channel, namely emergence and merging of liquid water on the GDL surface, accumulation on the sidewalls, and detachment from the top wall. The flow patterns can be characterized by the channel cross-sectional water distribution and coverage on the different walls. Water on the hydrophobic GDL surface tends to form droplets, while water on any of the hydrophilic surface tends to form a thin liquid film. The total pressure drop in the flow channel is mainly caused by droplet blockage of the channel by the droplet.

(2) The microstructure of the GDL surface has a significant impact on the two-phase flow patterns in the flow channel. The uniform inlet case and 1-pore case, approximations commonly used in previous studies, showed distinct flow patterns which are quite different from those observed in multiple pores. For the 4-pore, 16-pore and 64-pore cases, the flow patterns are similar, suggesting that the 4-pore case may be a minimum requirement to represent the microstructure of the GDL surface with a reasonable CPU time.

(3) The wettability of both the GDL surface and channel walls also has a significant influence on the two-phase flow patterns in the flow channel. It was shown that more hydrophobic GDL surface and/or more hydrophilic channel walls would be helpful to remove the liquid droplets from the GDL surface to the channel walls. Decreasing liquid water coverage of the GDL will facilitate the gas reactants diffusion through the GDL to the catalyst layer and should improve the PEM fuel cell performance.

(4) A lower liquid water flow rate into the channel can facilitate faster water removal due to the relatively faster detachment of water from the top wall. However, simulation results also show that the liquid flow rate has little influence on the two-phase flow patterns formed in the channel. Thus, in order to shorten the computational time, the liquid flow rates could be amplified by several orders of magnitude in order to study the flow characteristics qualitatively in operating fuel cells.

Acknowledgement

The authors are grateful to the Natural Science and Engineering Research Council of Canada (NSERC) for a Strategic Grant to support this study.

References

[1] A.Z. Weber, J. Newman, Chem. Rev. 104 (10) (2004) 4679–4726.
[2] C.Y. Wang, Chem. Rev. 104 (10) (2004) 4727–4765.
[3] A. Biylkoglu, Int. J. Hydrogen Energy 30 (11) (2005) 1181–1212.
[4] V. Gurau, J.A. Mann, SIAM J. Appl. Math. 70 (2) (2004) 410–454.
[5] R. Anderson, L.F. Zhang, Y.L. Ding, M. Blanco, X.T. Bi, D.P. Wilkinson, J. Power Sources 195 (15) (2010) 4531–4553.
[6] S. Um, C.Y. Wang, K.S. Chen, J. Electrochem. Soc. 147 (12) (2000) 4485–4493.
[7] S. Mazumder, J.V. Cole, J. Electrochem. Soc. 150 (11) (2003) A1503–A1509.
[8] A. Theodorakakos, T. Ous, M. Gavaises, J.M. Nouri, N. Nikolopoulos, H. Yanagihara, J. Colloid Interface Sci. 300 (2006) 673–687.
[9] Z.H. Wang, C.Y. Wang, K.S. Chen, J. Power Sources 94 (1) (2001) 40–50.
[10] T. Berning, N. Djilali, J. Electrochem. Soc. 150 (12) (2003) A1589–A1598.
[11] V. Gurau, J.A. Mann, Electrochem. Soc. 157 (4) (2010) B512–B521.
[12] Z. Zhan, J. Xiao, M. Pan, R. Yuan, J. Power Sources 160 (1) (2006) 1–9.
[13] E. Shirani, S. Masoomi, J. Fuel Cell Sci. Technol. 5 (4) (2008) 041008–41018.
[14] Y.H. Cai, J. Hu, H.P. Ma, B.L. Yi, H.M. Zhang, J. Power Sources 161 (2) (2006) 843–848.
[15] X. Zhu, P.C. Sui, N. Djilali, J. Power Sources 172 (1) (2007) 287–295.
[16] A. Bazylak, D. Sinton, N. Djilali, J. Power Sources 176 (1) (2008) 240–246.
[17] X. Zhu, P.C. Sui, N. Djilali, Microfluid. Nanofluid. 4 (6) (2008) 543–555.
[18] X. Zhu, P.C. Sui, N. Djilali, J. Power Sources 181 (1) (2008) 101–115.
[19] C. Fang, C. Hidrovo, F.-M. Wang, J. Eaton, K. Goodson, Int. J. Multiphase Flow 34 (2008) 690–705.
[20] P. Quan, B. Zhou, A. Sobiesiak, Z. Liu, J. Power Sources 152 (2005) 131–145.
[21] K. Jiao, B. Zhou, P. Quan, J. Power Sources 154 (1) (2006) 124–137.
[22] K. Jiao, B. Zhou, P. Quan, J. Power Sources 157 (1) (2006) 226–243.
[23] P. Quan, M.C. Lai, J. Power Sources 164 (1) (2007) 222–237.

[24] A.D. Le, B. Zhou, J. Power Sources 182 (1) (2008) 197–222.
[25] A.D. Le, B. Zhou, Electrochim. Acta 54 (8) (2009) 2137–2154.
[26] B. Markicevic, A. Bazylak, N. Djilali, J. Power Sources 171 (2) (2007) 706–717.
[27] J.T. Gostick, M.A. Ioannidis, M.W. Fowler, M.D. Pritzker, J. Power Sources 173 (1) (2007) 277–290.
[28] P.K. Sinha, C.Y. Wang, Electrochim. Acta 52 (28) (2007) 7936–7945.
[29] K.J. Lee, J.H. Nam, C.J. Kim, Electrochim. Acta 54 (4) (2009) 1166–1176.
[30] K. Schladitz, S. Peters, D. Reinel-Bitzer, A. Wiegmann, J. Ohser, Comput. Mater. Sci. 38 (1) (2006) 56–66.
[31] P.K. Sinha, P.P. Mukherjee, C.Y. Wang, J. Mater. Chem. 17 (30) (2007) 3089–3103.
[32] L. Hao, P. Cheng, J. Power Sources 186 (1) (2009) 104–114.
[33] J.U. Brackbill, D.B. Kothe, C. Zemach, J. Comput. Phys. 100 (2) (1992) 335–354.
[34] FLUENT 6.3 User's Guide, Fluent Inc., 2006.
[35] K.W. Morton, Numerical Methods for Fluid Dynamics (Institute of Mathematics and Its Applications Conference Ser), Academic Press, 1983.
[36] S. Litster, N. Djilali, in: B. Sunden, M. Faghri (Eds.), Transport Phenomena in Fuel Cells, WIT Press, 2005, pp. 175–213.
[37] L. Cindrella, A.M. Kannan, J.F. Lin, K. Saminathan, Y. Ho, C.W. Lin, J. Wertz, J. Power Sources 194 (1) (2009) 146–160.